Limnol. Oceanogr., 39(3), 1994, 609–631

A high resolution bio-optical model of microalgal growth: Tests using sea-ice algal community time-series data

Kevin R. Arrigo
Oceans and Ice Branch, Code 971, NASA/Goddard Space Flight Center, Greenbelt, Maryland 20771

Cornelius W. Sullivan
Graduate Program in Ocean Sciences, Hancock Institute for Marine Studies, University of Southern California, Los Angeles 90089-0373

Abstract

A high resolution, two-dimensional (z, t) time-dependent model of microalgal growth has been developed in which simulated physiological responses are determined by ambient temperature, spectral irradiance, nutrient concentration, and salinity. The model is based on the concept of a maximum temperature-dependent growth rate that is subsequently reduced by limitations imposed from insufficient light or nutrients, as well as sub- or supraoptimal salinity. Limitation terms for these variables are derived from studies of nutrient-, light-, and salinity-dependent algal growth (or photosynthetic) rates that have been normalized to maximum observed rates with respect to each variable. Particular emphasis was placed on developing the formulation for light limitation, which includes the effects of diel changes in spectral irradiance, seasonal changes in photoperiod, and related adjustments in biochemical C : Chl *a* ratios. This level of detail was needed because the importance of light limitation has been demonstrated on diurnal, seasonal, and annual time scales in polar regions. The model was tested by comparing simulation results to a sea-ice microalgal bloom in McMurdo Sound, Antarctica, in 1982. Environmental information from 1982 and biological coefficients derived from sea-ice communities were used as model input. Model results showed excellent agreement with microalgal bloom dynamics observed in 1982 under a variety of environmental conditions. Predicted Chl *a* standing crops were consistently within 15% of observations for the congelation ice and platelet ice, regardless of snow thickness (snow-free, 5-cm, and 10-cm snow-cover scenarios were tested), and predicted vertical distributions of Chl *a* exhibited the same depth-dependent pattern as observations.

Microalgae living in many aquatic ecosystems experience widely fluctuating environmental conditions which profoundly influence rates of photosynthesis and growth. For example, in upwelling regions, ambient irradiance and temperature may change on time scales of hours as seawater from depth is advected to the surface. Similarly, estuarine and sea-ice algal assemblages may experience rapid diel and seasonal shifts in salinity and temperature. Accurate assessments of primary production must accommodate the structural and physicochemical variability characteristic of these habitats; consequently, the tendency has been for models of algal growth to increase in complexity. Early models simply predicted primary production from distributions of light and chlorophyll (Ryther 1956). However, because the photosynthetic characteristics of phytoplankton vary with depth, time of day, season, and region, these models were found to be too simplistic. Later models incorporated the effects of presumed depth-dependent changes in photosynthetic parameters (i.e. quantum yield) on productivity (Laws and Bannister 1980; Kiefer and Mitchell 1983; Smith et al. 1989). Eventually, the influence of nutrients and temperature on phytoplankton growth and biochemical composition was also included (Kiefer and Cullen 1991; Sakshaug et al. 1991). Other models incorporated the effects of spectral irradiance (Sathyendranath 1989; Morel 1991; Platt and Sathyendranath 1991) and daylength (Sakshaug et al. 1991). In some cases, diel changes in irradiance were also included (Wroblewski 1977;

Acknowledgments

We thank Mike Lizotte, Steve Ackley, Jim Kremer, Dale Kiefer, John Cullen, and an anonymous reviewer for comments on earlier versions of this manuscript. We are also grateful to Dale Robinson and Mike Lizotte for helpful insights during the formulation of this model. We are particularly appreciative of the manner in which Susan Kilham handled all facets of the publication of this manuscript.

This work was supported by NSF grants DPP 87-17692 (Division of Polar Programs) to C. W. Sullivan and by a U.S. Department of Energy Global Change Distinguished Postdoctoral Fellowship to K. Arrigo and administered by Oak Ridge Institute for Science and Education.

Platt et al. 1990; Platt and Sathyendranath 1991).

Unfortunately, few models account for the effects of more than two environmental factors in their formulations of phytoplankton growth. For instance, Kiefer and Mitchell (1983) and Wroblewski and Richman (1987) used photosynthetically active radiation (PAR) and nutrient concentrations to model phytoplankton growth. Sakshaug et al. (1991) utilized only spectral irradiance and daylength. The model of Smith et al. (1989) is somewhat more complex, simulating the effects of spectral irradiance, daylength, and diel changes in irradiance. A more sophisticated model has recently been developed by Kiefer and Cullen (1991). It includes the effects of PAR, daylength, nutrients, and temperature, although it ignores the spectral distribution of and diel changes in irradiance.

A recent paper by Arrigo et al. (1993*a*) describes a two-dimensional (depth and time) coupled physical-biological ecosystem model of Antarctic landfast ice. This model emphasizes the influence of dynamical changes in sea-ice growth, internal structure, and chemistry on microalgal growth within sea ice. Here, we present in detail the biological component of that model, focusing on the physiological responses of ice microalgae to changes in environmental forcing, including temperature, diel variation in spectral irradiance, concentrations of inorganic macronutrients (nitrate, ammonium, phosphate, and silicic acid), and salinity. To our knowledge, this is the first time that all of these factors have been included in a single formulation of microalgal growth.

The model

Microalgal growth—Microalgal growth rates in the model are determined by calculating the maximum temperature-dependent rate and then multiplying this by dimensionless coefficients which represent the effect of resource limitation (nitrogen, silicon, phosphorus, or light) and sub- or supraoptimal salinity (Arrigo and Sullivan 1992). Eppley (1972) suggested that the maximum temperature-dependent rate of phytoplankton growth (nonlimited), μ_{max}, is described by

$$\mu_{max}(z) = \mu_0 \exp[r_\mu T(z)]. \quad (1)$$

μ_0 is the specific growth rate at 0°C, r_μ is a rate constant that determines the sensitivity of μ_{max} to changes in temperature, and $T(z)$ is temperature at depth z. (Units given in list of notation.) Eppley (1972) determined μ_0 to be 0.8511 and r_μ to be 0.0633 based on the growth of various phytoplankton species acclimated to temperatures >2°C. This formulation also appears to adequately describe algal growth at lower temperatures (Grossi et al. 1984; Spies 1987; Robinson 1992).

The rate of algal growth is determined by the availability of a single most-limiting resource (Blackman 1905). This resource may be either light or a nutrient (such as nitrate, silicic acid, or phosphate). The empirical formulation of Monod (1942) is commonly used to identify the most-limiting nutrient, despite its limitations (Williams 1973). The Monod formulation is expressed as

$$\mu(z) = \mu_{max}(z)\frac{N_i(z)}{K_s + N_i(z)}. \quad (2)$$

$\mu(z)$ is the specific growth rate, $N_i(z)$ is the concentration of nutrient i (e.g. ammonium, nitrate, silicic acid, or phosphate) at depth z, and K_s is the temperature-independent half-saturation constant for N_i defined as the concentration where $\mu = \mu_{max}/2$. Obtaining a dimensionless N_i-limitation coefficient requires Eq. 2 to be rewritten as

$$\left(\frac{\mu}{\mu_{max}}\right)_i(z) = \frac{N_i(z)}{K_s + N_i(z)}. \quad (3)$$

$(\mu/\mu_{max})_i(z)$ describes the fraction of the temperature-dependent growth rate allowed by N_i at depth z. Because K_s is assumed to be independent of temperature and μ_{max} is not, μ at a given growth-limiting N_i will be temperature-dependent (Maddux and Jones 1964). Equation 3 is used to determine $N_{lim}(z)$, the nutrient limitation coefficient for depth z, by evaluating which nutrient yields the minimum value for $(\mu/\mu_{max})_i(z)$. Therefore,

$$N_{lim}(z) = \text{Min}\left(\frac{\mu}{\mu_{max}}\right)_i(z). \quad (4)$$

Because inorganic N occurs predominantly as ammonium and nitrate, the nitrogen source which is least limiting to microalgal growth (as determined by Eq. 3) will be used in Eq. 4.

Several models include separate formulations for describing light and nutrient-limited algal growth (i.e. Shuter 1979; Laws and Ban-

Notation

a	Fraction of grazed C that is assimilated, dimensionless	N_{lim}	Fraction of μ_{max} allowed by nutrients, dimensionless
a_{max}	Microalgal absorption coefficient at 440 nm, m^{-1}	PAR, PUR	Photosynthetically available and usable radiation (400–700 nm), μEinst m^{-2} s^{-1}
$a^*(\lambda)$	Pigment-specific absorption coefficient, m^2 (mg Chl a)$^{-1}$	P^B, P^B_s	Chl a-specific photosynthetic rate and maximum Chl a-specific photosynthetic rate, mg C (mg Chl a)$^{-1}$ h^{-1}
$a_d(\lambda)$, $a_m(\lambda)$	Detritial and microalgal absorption coefficient, m^{-1}	r_r, r_μ	Sensitivity of R and μ to temperature, T^{-1}
A, B	Coefficients to calculate I_k, dimensionless	r_{lim}	Fraction of μ_{max} allowed by available resources, dimensionless
C	Carbon, mmol m^{-3}	R, R_0	Microalgal and specific respiration rate at 0°C, d^{-1}
D	Photoperiod, h	R_{sky}, R_{sun}	Fraction of diffuse and direct irradiance reflected at the surface, dimensionless
e	Fraction of assimilated C that is excreted, dimensionless	S_b	Brine salinity, ‰
E	Excretion rate, d^{-1}	t	Time, h
$E_d(\lambda)$	Total downwelling irradiance, μEinst m^{-2} s^{-1} nm^{-1}	T	Temperature, °C
$E_{dsky}(\lambda)$, $E_{dsun}(\lambda)$	Diffuse and direct downwelling irradiance, μEinst m^{-2} s^{-1} nm^{-1}	z	Depth, m
g	Fraction of net positive production that is grazed, dimensionless	α^B	Chl a-specific photosynthetic efficiency, mg C (mg Chl a)$^{-1}$ h^{-1} (μEinst m^{-2} s^{-1})$^{-1}$
G	Grazing rate, d^{-1}	λ	Wavelength, nm
H	Sea-ice thickness, m	ρ	Fraction of μ_{max} allowed by light, dimensionless
H_p	Platelet-ice depth, m	μ, μ_0, μ_{max}	Specific microalgal growth rate, specific microalgal growth rate at 0°C, and maximum specific microalgal growth rate, d^{-1}
I_k	Photoadaptation parameter, μEinst m^{-2} s^{-1}	ç	C:Chl a at PAR/C:Chl a at I_k, dimensionless
I_k', $I_k'_{max}$	Spectral photoadaptation parameter and maximum spectral photoadaptation parameter, μEinst m^{-2} s^{-1}	ξ	Fraction of μ_{max} allowed by salinity, dimensionless
$K_d(\lambda)$	Downwelling attenuation coefficient, m^{-1}	Γ	Nutrient transport coefficient, m^2 d^{-1}
$K_{di}(\lambda)$, $K_{dp}(\lambda)$	Downwelling attenuation coefficient for sea ice and for particles, m^{-1}.		
$K_s(\lambda)$	Half-saturation constant for N_i uptake, μM		
M	Microalgae, mmol C m^{-3}		
N_i	Concentration of nutrient i, mmol m^{-3}		

nister 1980; Kiefer and Mitchell 1983). The formulation for light limitation chosen here has three key advantages over other models of light-limited algal growth: it is based on a single photosynthetic parameter, I_k'; it includes changes in spectral irradiance distribution over depth z due to attenuation by the medium and by algal pigments; and it accounts for the diel variation in spectral irradiance.

Numerous formulations have been developed to describe the functional relationship between photosynthetic rate and incident irradiance (PI). In most cases, photosynthetically active radiation (PAR), computed as

$$\mathrm{PAR}(z, t) = \int_{\lambda=400}^{700} E_d(z, t, \lambda)\, d\lambda \qquad (5)$$

where $E_d(z, t, \lambda)$ is the downwelling spectral irradiance at time t and depth z, was used. Most PI formulations incorporate separate terms to describe light-limited and light-saturated photosynthetic rates; some also include a term which describes reduced rates of photosynthesis at high light due to photoinhibition (e.g. Platt et al. 1980). We use the PI model developed by Platt et al. (1980) and neglect photoinhibition. Consequently,

$$P^B(z, t) = P^B_s \left\{ 1 - \exp\left[- \frac{\alpha^B \mathrm{PAR}(z, t)}{P^B_s} \right] \right\}. \qquad (6a)$$

$P^B(z, t)$ is the instantaneous biomass-specific photosynthetic rate at depth z, P^B_s is the light-saturated photosynthetic rate, and α^B is the photosynthetic efficiency defined by the initial slope of the PI curve.

Equation 6a can be rewritten in terms of the photoadaptation parameter, I_k ($= P_s^B/\alpha^B$ in the absence of photoinhibition):

$$P^B(z, t) = P_s^B\left\{1 - \exp\left[-\frac{\mathrm{PAR}(z, t)}{I_k(z)}\right]\right\}. \quad (6b)$$

$I_k(z)$ is assumed to remain constant for a given day. To derive a dimensionless coefficient for light-limited algal growth from Eq. 6b requires moving P_s^B to the left side of the equation and adding a factor that corrects for the expected C:Chl *a* ratio differences at the light levels PAR(z) and $I_k(z)$. Thus,

$$\rho(z, t) = 1 - \exp\left[-\frac{\mathrm{PAR}(z, t)}{I_k(z)}\,ç\right]. \quad (6c)$$

$\rho(z, t) = P^B(z, t)/P_s^B$, and

$$ç = \frac{\text{cellular C:Chl } a \text{ for algae at PAR}(z)}{\text{cellular C:Chl } a \text{ for algae at } I_k(z)}. \quad (7)$$

A rigorous description of the relationship between the cellular C:Chl *a* ratio and light level is unavailable for sea-ice microalgae; therefore, we used data for *Skeletonema costatum* (Sakshaug et al. 1989) instead. A reanalysis of the data of Sakshaug et al. (1989) shows that at high growth rates (where nutrients are in abundance), C:Chl *a* is a function of daily integrated radiation (Einst m^{-2} d^{-1}, the product of the photoperiod, D, and PAR) of the form (Fig. 1A):

$$\text{cellular C:Chl } a = 33.125 + 9.77\,D \times \mathrm{PAR}. \quad (8)$$

Although this relationship is based on the response of a phytoplankton species, the minimum C:Chl *a* ratio from Eq. 8 is consistent with that of sea-ice microalgae (Palmisano and Sullivan 1983; Palmisano et al. 1985; Arrigo unpubl.).

One disadvantage of Eq. 6c is that it neglects the effects of spectral irradiance shifts. As light is transmitted through sea ice (or water), it is shifted toward the blue region of the spectrum where it can be absorbed readily by algal pigments (Sathyendranath et al. 1989; Arrigo et al. 1991). However, selective absorption by microalgae can shift peak irradiance toward the green wavelengths, resulting in an irradiance distribution of reduced spectral quality. Therefore, PAR in Eq. 6c has been replaced by photosynthetically usable radiation (PUR). PUR differs from PAR in that it is a measure of the available radiation between 400 and 700 nm that can be readily absorbed by algae (Morel 1978). PUR is dependent on the absorption properties of the algal community as well as the spectral distribution of downwelling irradiance and is defined as

$$\mathrm{PUR}(z, t) = \int_{\lambda=400}^{700} E_d(z, t, \lambda)\frac{a_m(\lambda)}{a_{\max}}\,d\lambda \quad (9)$$

(Morel 1978). $a_m(\lambda)$ is an absorption spectrum for the microalgal sample, $a_{\max}$ is the absorption maximum between 400 and 700 nm, and $E_d(z, t, \lambda)$ is the ambient downwelling spectral irradiance. Consistency is maintained in Eq. 6c by converting PAR measured during incubations to PUR using the spectral characteristics of the incubator light source and $a_m(\lambda)$. This spectral modification yields a PUR-dependent value for I_k, hereafter referred to as I_k'. By considering the spectrally dependent parameters PUR and I_k' rather than PAR and I_k, the instantaneous light limitation term given in Eq. 6c is rewritten as

$$\rho(z, t) = 1 - \exp\left[-\frac{\mathrm{PUR}(z)}{I_k'(z)}\,ç\right]. \quad (10)$$

Estimates of the instantaneous light-limited photosynthetic rate can be extended to calculate light limitation on a daily basis. Such a calculation requires a time-varying estimate of PUR(z, t) during the photoperiod, D. Diel changes in PUR(z, t) are represented as a sinusoidal function of t, where t varies from 12 $- D/2$ to 12 $+ D/2$. In this scheme, PUR(z, t) is calculated from PUR(z) at noon and midnight [referred to as PUR(z, 12) and PUR(z, 24), respectively] and D with the equation

$$\mathrm{PUR}(z, t) = \frac{\mathrm{PUR}(z, 12) + \mathrm{PUR}(z, 24)}{2} - \frac{\mathrm{PUR}(z, 12) - \mathrm{PUR}(z, 24)}{2} \times \cos\left[\frac{2\pi(t - 12 + D/2)}{D}\right]. \quad (11)$$

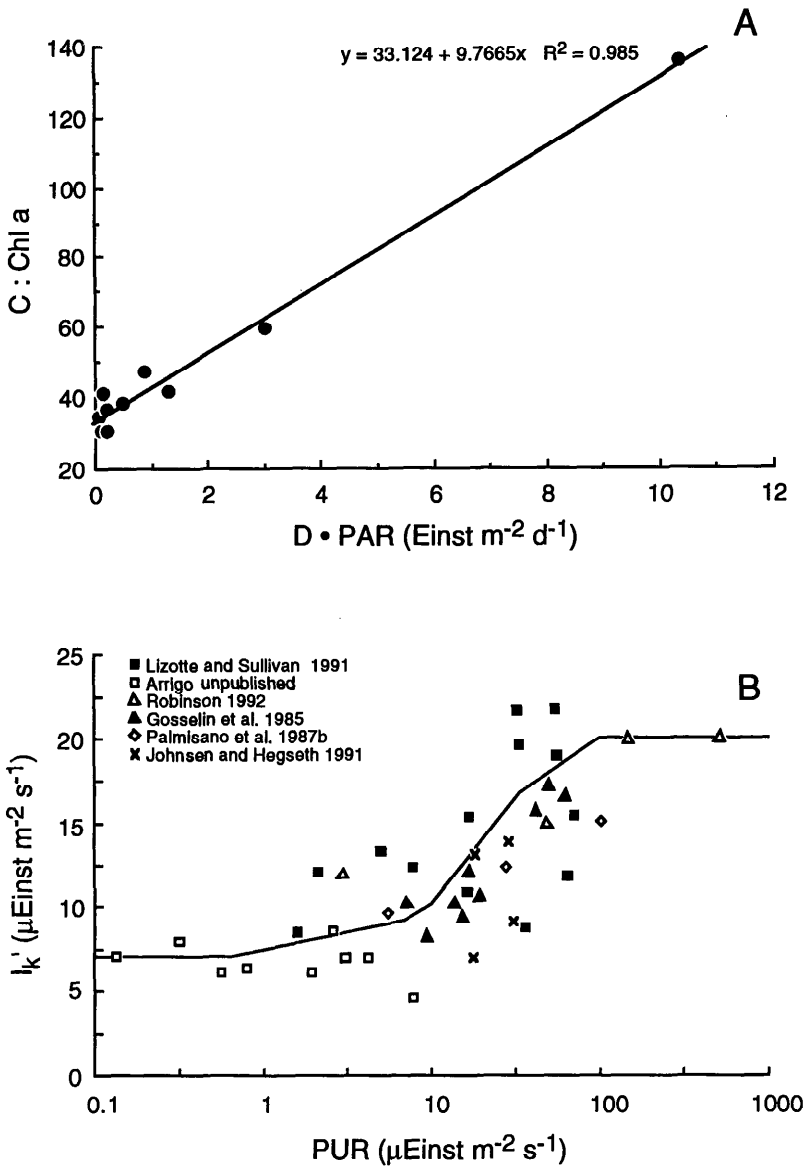

Fig. 1. A. Biochemical C:Chl *a* ratio for *Skeletonema costatum* vs. daily integrated radiation, calculated as the product of the photoperiod, *D*, and PAR, which was held constant during *D*. Data are from Sakshaug et al. (1989); only experiments exhibiting high growth rates (high nutrients) at a particular *D* and PAR combination were used in the analysis. B. I_k' vs. PUR. I_k' was assumed to be 50% of the I_k determined from PI analysis when tungsten-halogen incubator light sources were used, 60% when "cool-white" fluorescent lights were used, and 70% when blue filters were used. PUR was calculated from Eq. 9 with the light spectra to which ice microalgae were acclimated. If PI analyses were performed immediately after collection, PUR was assumed to be 35% of the reported PAR value. The best-fit equation describing the shape of the solid curve is $I_k' = 18/[1 + 1.7 \exp(-0.12\ \mathrm{PUR})]$.

Figure 2 illustrates the ability of Eq. 11 to accurately represent diel changes in irradiance.

$I_k'(z)$ and daily variation in PUR(z,t) are used to estimate the daily depth-dependent light-limitation coefficient, $\rho(z)$:

$$\rho(z) = \frac{\int_{t=12-D/2}^{12+D/2} 1 - \exp\left[-\frac{\mathrm{PUR}(z,\ t)}{I_k'(z)}\ \text{ç}\right] \mathrm{d}t}{\int_{t=0}^{24} \mathrm{d}t}; \qquad (12)$$

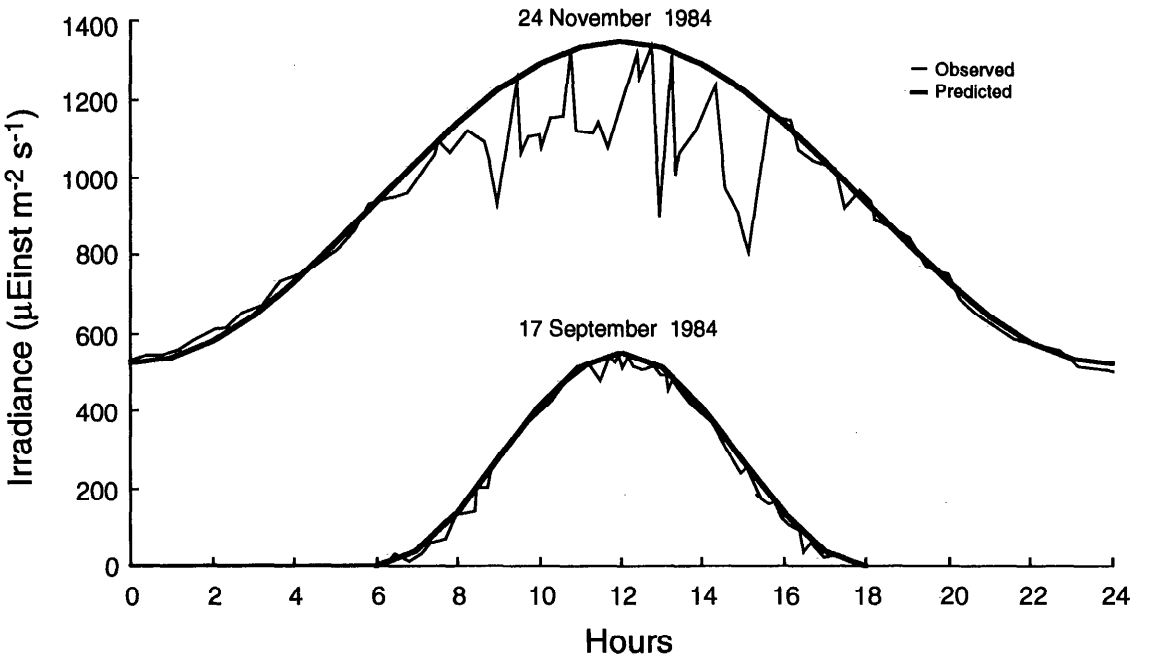

Fig. 2. Comparison of diel variations of atmospheric PAR measured in McMurdo Sound in 1984 with predictions made with Eq. 11 after replacing PUR(z, t) with PAR(z, t).

the numerator of Eq. 12 varies between 0 and 24, and the denominator is equal to 24.

The relative magnitudes of PUR(z, t) and I_k' fall into three distinct categories. Case 1 describes the situation when PUR(z, t) is constantly $< I_k'(z)$ and the algae are light-limited throughout the day. Case 2, which could occur naturally in polar regions, is characterized by oscillations of PUR(z, t) around $I_k'(z)$, and the algae are light-limited for only portions of the day. Case 3 is when PUR(z, t) is always $> I_k'(z)$ and the algae are never light limited.

The value of $\rho(z)$ ultimately depends on the magnitude of I_k'. The photoadaptation parameter reflects the balance between dark and light reactions (Falkowski 1981) and, as mentioned earlier, is a derived parameter calculated as

$$I_k = P_s^B/\alpha^B.$$

The value of the parameters used to calculate I_k' can be difficult to predict for a specific environment because of the dependence of P_s^B on nutrient supply, light history, temperature, and daylength, and the dependence of α^B on light history and nutrient availability. For this reason, we have estimated empirical values for I_k' which are based on the observed relationship between I_k' and mean daily PUR for sea-ice microalgae collected primarily from McMurdo Sound, Antarctica. Unfortunately, estimating I_k' in this way precludes daily variation—a phenomenon observed in numerous studies (e.g. Harding et al. 1982; Rivkin and Putt 1988). The relationship between I_k' and mean daily PUR, shown in Fig. 1B, is described by the logistic equation

$$I_k' = \frac{I_{k'\max}}{1 + A \exp(-B \text{ PUR})}. \quad (13)$$

A is 1.7 and B is 0.12; $I_{k'\max}$ = 18 μEinst m^{-2} s^{-1}. We chose the logistic equation because it allows I_k' to reach asymptotic values at very low and very high irradiances, a pattern strongly suggested by the data. Because PUR in Fig. 1B is intended to represent a relatively long-term mean, the model calculates PUR for input to Eq. 13 as a 3-d moving average of PUR(z, t). This invariably results in a case 2 situation during simulations.

The data used to create Fig. 1 require some explanation. Whenever possible, I_k' was computed from measurements of photosynthesis

where PUR was held constant for several days before I_k' was determined. In studies where PI analyses were performed soon after collection of algal samples, microalgae were assumed to be acclimated to the light levels reported in conjunction with the values for I_k. Although we do not know whether the growth of ice microalgae collected during these studies was balanced, this assumption is most defensible for attached algal species growing at high latitudes where photoperiod may be 24 h and diel changes in irradiance are much smaller than typically observed at lower latitudes. It must be noted, however, that even in McMurdo Sound, surface irradiance may vary by as much as 800 μEinst m^{-2} s^{-1} between noon and midnight under clear skies (Fig. 2), although variability will be much lower under sea ice. Low correlations between PUR and I_k' (as evidenced by the scatter in Fig. 1B) can arise when instantaneous measurements of irradiance are reported that do not adequately reflect the light history in situ of the algal assemblage, or when the spectral light field used for the estimation of PUR is not well described. In addition, sampling during the studies of Robinson (1992), Arrigo (unpubl.), and Gosselin et al. (1985) was restricted to a single site and exhibited tighter correlations than data from Lizotte and Sullivan (1991) and Johnsen and Hegseth (1991), who sampled multiple sites.

Once the limitation due to light and individual nutrients has been assessed, the most limiting resource at depth z is determined by the relation

$$r_{\text{lim}}(z) = \text{Min}[N_{\text{lim}}(z);\ \rho(z)]. \qquad (14)$$

$r_{\text{lim}}(z)$ is equivalent to the smaller of the nutrient-, $N_{\text{lim}}(z)$, and light-, $\rho(z)$, limitation terms.

At thermal equilibrium, the salinity of sea-ice brine (S_b) is determined directly by temperature; thus, colder temperatures at the upper sea-ice surface result in higher S_b values. Salinity can have a substantial impact on rates of algal photosynthesis and growth (Grant and Horner 1976; Bates and Cota 1986) and appears to act independently of both temperature and resource limitation (Arrigo and Sullivan 1992). The salinity-dependent values for P_s^B given by Arrigo and Sullivan (1992) (Fig. 3A) have been normalized to the highest P_s^B measured at any salinity (Fig. 3B) to obtain a coefficient capable of mathematically describing the relationship between salinity and algal growth. The salinity-dependent growth coefficient, $\xi(z)$, at a given depth z was determined by the least-squares polynomial fit to the data shown in Fig. 3B:

$$\xi(z) = \alpha_1 + \alpha_2 S_b(z) + \alpha_3 S_b(z)^2 + \alpha_4 S_b(z)^3 + \alpha_5 S_b(z)^4 + \alpha_6 S_b(z)^5. \qquad (15)$$

$S_b(z)$ is the brine salinity at depth z, $\alpha_1 = 1.1 \times 10^{-2}$, $\alpha_2 = 3.012 \times 10^{-2}$, $\alpha_3 = 1.034 \times 10^{-3}$, $\alpha_4 = 4.6033 \times 10^{-5}$, $\alpha_5 = 4.926 \times 10^{-7}$, and $\alpha_6 = 1.659 \times 10^{-9}$.

Because, when considered together, the independent effects of temperature, salinity, and resource limitation act multiplicatively to control algal growth (Arrigo and Sullivan 1992), Eq. 1, 14, and 15 can be combined to yield the final gross growth equation

$$\mu(z) = \mu_{\text{max}}(z) r_{\text{lim}}(z) \xi(z) \qquad (16)$$

where $\mu(z)$ is the predicted gross algal growth rate (d^{-1}). This equation represents the first attempt to incorporate the effects of temperature, salinity, nutrients, and diel changes in spectral irradiance into a physiological model of microalgal growth.

Microalgal respiration—The temperature-dependent rate of microalgal respiration, R, is calculated in much the same way as growth with the equation

$$R(z) = R_0 \exp[r_r T(z)] \qquad (17)$$

(Riley 1946). $R(z)$ is the specific respiration rate at depth z, R_0 is the specific respiration rate at 0°C, and $T(z)$ is temperature at depth z. When $R_0 = 0.05$ and $r_r = 0.0633$, total daily respiratory losses are ~10% of gross growth rate, consistent with both our understanding of dark respiration by microalgae growing under light-limited conditions (Geider 1992) and with field estimates for phytoplankton respiratory losses (Yentsch 1981).

Other biological dynamics—Due to the uncertainty regarding grazing processes in sea-ice ecosystems, the magnitude of the grazing rate, $G(z)$, has simply been assumed to be a constant fraction, g, of any positive net production such that

$$G(z) = g[\mu(z) - R(z)]. \qquad (18)$$

The rate of NH_4 excretion, E, by micro- or macrozooplankton is assumed to be related to G and the assimilated fraction, a, by the equation

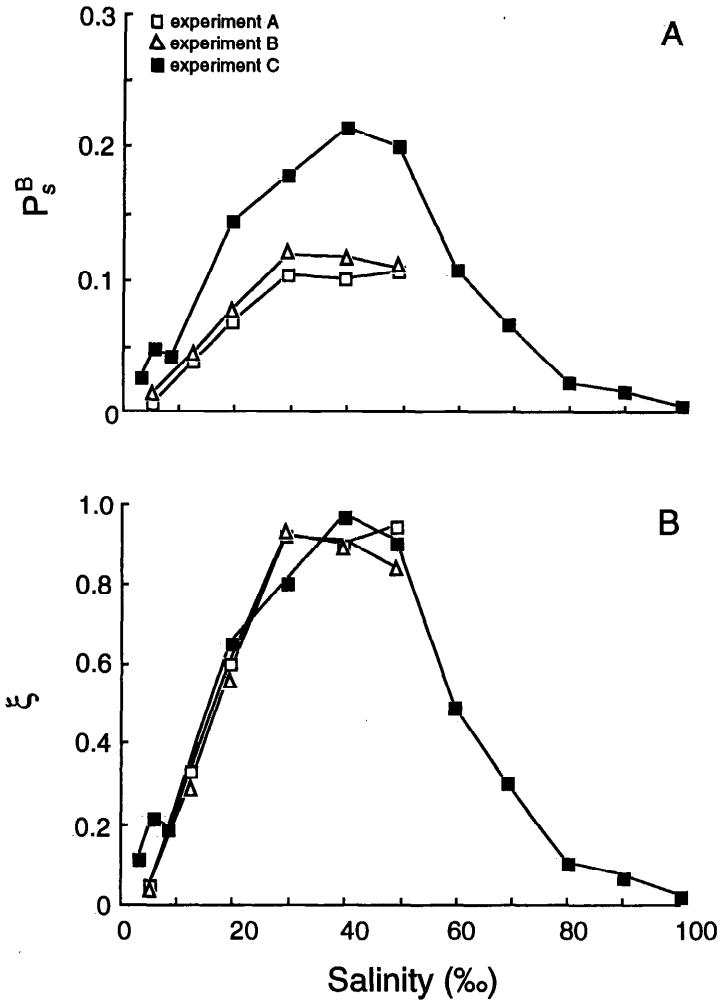

Fig. 3. A. The relationship between P_s^B [mg C (mg Chl a)$^{-1}$ h^{-1}] and salinity for ice microalgae collected in McMurdo Sound. B. Same data as in panel A but normalized to the maximum assimilation rate for each experiment to obtain the dimensionless salinity coefficient, ξ. Experiments A and B were performed in 1988, experiment C in 1989. (Data from Arrigo and Sullivan 1992).

$$E(z) = eaG(z) \tag{19}$$

where e is the fraction of the assimilated carbon that is excreted.

The final set of biological equations is defined as

$$\frac{\partial M(z)}{\partial t} = M(z)[\mu(z) - R(z) - G(z)], \tag{20}$$

and

$$\frac{\partial N_i(z)}{\partial t} = M(z)\frac{N_i}{C}\{E(z) - [G(z) - R(z)]\}. \tag{21}$$

M is the microalgal biomass, and N_i:C is the molar ratio of nutrient i to carbon.

Physical dynamics—The present biological model has been coupled to a simple two-dimensional (z, t) model of first year sea-ice structure and dynamics that incorporates the effect of radiative transfer (including cloud cover), sea-ice growth, desalination, and nutrient flux and describes the physicochemical features of the ice sheet (Arrigo et al. 1993*a*). Radiative transfer formulations used in this model are summarized below and described in detail by Arrigo et al. (1991). Equations de-

scribing the other physical processes which are important to algal growth in sea ice are presented by Arrigo et al. (1993*a*).

Spectral downwelling irradiance just beneath the surface of the ice (or snow, if present), $E_d(0, \lambda)$, is the sum of the direct, $E_{d\text{sun}}(0, \lambda)$, and diffuse, $E_{d\text{sky}}(0, \lambda)$, components after accounting for specular reflection (R_{sun} and R_{sky}, respectively). The equation used to describe this relationship is

$$E_d(0, \lambda) = (1 - R_{\text{sun}})E_{d\text{sun}}(0, \lambda) + (1 - R_{\text{sky}})E_{d\text{sky}}(0, \lambda). \quad (22)$$

$R_{\text{sky}} = 0.05$, and R_{sun} is a function of sun angle as determined by Snell's law. $E_d(0, \lambda)$ is attenuated by snow or ice according to the Beer-Lambert law:

$$E_d(z, \lambda) = E_d(0, \lambda) \exp[-K_d(z, \lambda)\, z]. \quad (23)$$

z is depth, and $K_d(z, \lambda)$ is the spectral downwelling attenuation coefficient. In the case of snow, $K_d(z, \lambda)$ is determined by the attenuation coefficient of snow alone, $K_{ds}(z, \lambda)$; for sea ice, $K_d(z, \lambda)$ is determined from the attenuation coefficients of the ice (K_{di}) and any particles (K_{dp}) present, such that

$$K_d(z, \lambda) = K_{di}(z, \lambda) + K_{dp}(z, \lambda). \quad (24)$$

$K_{di}(\lambda)$ is determined by the brine volume of the ice sheet, which is a function of temperature, and $K_{dp}(\lambda)$ is calculated as

$$K_{dp}(z, \lambda) = \frac{a_m(z, \lambda) + a_d(z, \lambda)}{\bar{\mu}}. \quad (25)$$

$a_m(z, \lambda)$ and $a_d(z, \lambda)$ are the absorption coefficients for microalgae and detritus (backscattering by ice particles has been ignored), and $\bar{\mu}$ (0.656) is the mean cosine of the angular irradiance distribution within sea ice. Due to the highly scattering nature of sea ice, $\bar{\mu}$ varies somewhat in the upper few centimeters of the ice sheet but rapidly approaches a constant asymptotic value of 0.656 with depth. Microalgal absorption is determined by the pigment-specific absorption coefficient, $a^*(z, \lambda)$, and the concentration of Chl *a*, such that

$$a_m(z, \lambda) = a^*(z, \lambda)\text{Chl } a(z). \quad (26)$$

The values for $K_{ds}(\lambda)$, $K_{di}(\lambda)$, $a^*(\lambda)$, and $a_d(\lambda)$ used in the model are given by Arrigo et al. (1991).

Testing the model—The landfast sea-ice ecosystem in McMurdo Sound is an ideal environment in which to test the ability of the present model to simulate algal growth under variable environmental conditions. Microalgae growing in sea ice are exposed to wide seasonal fluctuations in temperature, salinity, and nutrient concentrations (Arrigo et al. 1993*a*), as well as large diel changes in the magnitude and spectral distribution of downwelling irradiance (Arrigo et al. 1991). During the spring bloom in 1982, sea-ice temperatures in September ranged from −1.86°C at the ice–water interface to <−30°C at the air–ice interface. On a seasonal basis, the depth-averaged temperature of the ice sheet increased from −10°C on 1 September to −3°C on 31 December (Fig. 4A). This temperature increase reduced the depth-averaged brine salinity from 140 to 50‰ within the congelation ice sheet (Fig. 4B). Surface PAR also exhibited dramatic seasonal changes, with daily maxima increasing from 200 μEinst m^{-2} s^{-1} on 1 September to 1,370 μEinst m^{-2} s^{-1} on 21 December (Fig. 4C). Congelation ice thickness increased by as much as 0.5 m during the spring bloom in 1982 (Fig. 4D), offsetting part of the seasonal increase in surface irradiance.

In addition to its physical and chemical variability, the sea-ice matrix provided a vertically stable surface for microalgal attachment and subsequent growth, removing the influence of vertical mixing on photoacclimation processes. The presence of a layer of platelet ice 0.5–1.0 m thick that forms beneath the congelation ice (Dieckmann et al. 1992) also reduces greatly the loss of algal biomass due to sinking and macrozooplankton grazing (Meguro et al. 1967; Grossi et al. 1987). Preliminary model results (Arrigo et al. 1993*b*) suggest that net production is grazed with 100% efficiency ($g = 1$) at depths ranging from the upper congelation ice surface to 20 cm above the congelation-ice/platelet-ice interface and with zero efficiency ($g = 0$) in the lower 20 cm of the congelation-ice and in the platelet-ice layer (except where noted).

With the exception of Si, the molar ratios for C : N : Si : P of 107 : 17 : 40 : 1 observed for sea-ice algae growing in McMurdo Sound (Arrigo and Gosselin unpubl.) agree reasonably well with previous estimates by Redfield (1958)

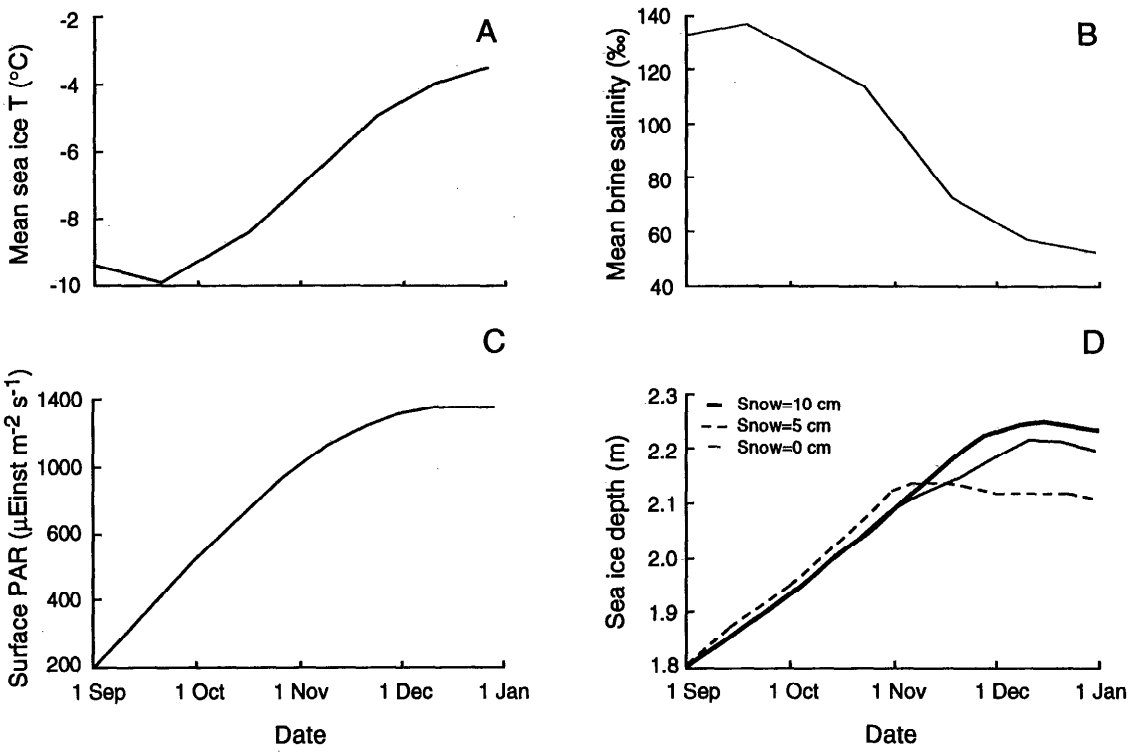

Fig. 4. Seasonal changes in mean temperature for the ice sheet (A), mean brine salinity for the ice sheet (B), surface PAR (C), and sea-ice thickness under various snow covers (D) in McMurdo Sound in 1982.

of 106 : 16 : 17 : 1 for phytoplankton. Therefore, the former ratios were used as default values in the model (Table 1). An extensive evaluation of the influence of using a lower C : Si ratio is provided by Arrigo et al. (1993*b*).

K_s values for sea-ice microalgae collected from McMurdo Sound have been measured at 0.3 μM for the uptake of NO_3, 0.2 μM for NH_4, 2.3 μM for PO_4, and >100 μM for $^{68}Ge(OH)_4$ (an analog for silicic acid, Azam et al. 1974) (Sullivan et al. unpubl.). The K_s for NO_3 is within the range of 0.1–0.5 μM reported for temperate planktonic diatoms (Falkowski 1975) and 0.3–4.2 μM for Antarctic planktonic diatoms (Sommer 1986). Sommer (1986) observed K_s for $Si(OH)_4$ uptake in the Antarctic diatoms *Corethron criophilum* and *Nitzschia kergulensis* of 60.1 and 88.7 μM—similar to values observed by Sullivan et al. (unpubl.). In contrast, the K_s for phosphate uptake obtained by Sullivan et al. (unpubl.) was much higher than previous estimates. K_s values used as defaults in the model were 1 μM nitrate, 1 μM ammonium, 60 μM silicic acid, and 0.1 μM phosphate (Table 1). Again, the effect of a high K_s for $Si(OH)_4$ uptake on model results was investigated by Arrigo et al. (1993*b*).

The sea-ice thickness, salinity and Chl *a* profiles, and nutrient concentrations must be specified at the start of each simulation. Default values used in the model were based on historical data collected from McMurdo Sound. Initial ice thickness was assumed to be 1.8 m—the mean thickness observed in McMurdo Sound between 1971 and 1989. The default vertical profiles of sea-ice salinity and Chl *a* were chosen to represent typical profiles observed in the fast ice of Antarctica (Sullivan unpubl.) and are reported in Table 1. Initial nutrient concentrations in the ice sheet are assumed to be conservative with salinity and proportional to concentrations in seawater. In the water column of McMurdo Sound in 1989, salinity averaged 34.5‰ while NO_3, NH_4, $Si(OH)_4$, and PO_4 concentrations averaged 30, 0.5, 75, and 2 μM (Dieckmann et al. 1992).

Results and discussion

Model validation: McMurdo Sound, 1982— We have compared model results to the dynamics of an algal bloom observed in McMurdo Sound during spring 1982. This particular year was chosen because studies undertaken at that time (i.e. Grossi et al. 1987; Palmisano et al. 1987*b*; Kottmeier et al. 1987) provide much of the biological and environmental information needed to define terms in our model and to test the model output against data collected in situ. The data set includes initial Chl *a* concentrations, seasonal changes in Chl *a* standing crop, thicknesses of congelation and platelet ice (Table 2), and snow depth. In addition, seasonal changes in algal standing crop in both the congelation ice and the platelet ice were monitored beneath 100-m^2 quadrats maintained under 0, 5, and 10 cm of snow cover (Grossi et al. 1987). Time-series data on air temperature and relative cloud cover were published in the *Antarctic Journal of the United States* (Table 2). We chose to focus on the temporal dynamics of the microalgal standing crop for model validation because this parameter conveniently integrates the effects of variations in growth rate with depth in the ice sheet. However, vertical profiles of Chl *a* from cores of congelation ice were also used for model validation whenever possible (platelet-ice profiles were not collected).

Simulated Chl *a* dynamics in the congelation ice (Fig. 5) and platelet ice (Fig. 6) show good agreement with observed dynamics in sea ice beneath 0, 5, and 10 cm of snow during the spring bloom. In the congelation ice, simulated specific rates of Chl *a* accumulation beneath 0, 5, and 10 cm of snow are within 1, 3, and 37% of observed rates (Table 3). Likewise, simulated Chl *a* accumulation rates in platelet ice beneath 0 and 5 cm of snow are within 7 and 12% of observations (Table 3). Regressing observed Chl *a* in the congelation and platelet ice under all snow conditions against the appropriate simulated values (Fig. 7A) demonstrates that the model was able to explain 96% of the observed variation in microalgal standing crop (the three points in the box shown in Fig. 7A were not included in the regression for reasons explained below). The decrease in model performance at greater snow thicknesses may be due to erroneous snow thickness measurements (an error of a few centimeters can have a severe impact on simulated algal growth), to problems with simulating the light field beneath snow whose thickness has been artificially manipulated, or to uncertainty in the optical properties of snow assumed by the model. If the latter is true, model results will be improved as our understanding of radiative transfer in snow increases. In any case, the agreement between observed and predicted algal growth rates under snow-free conditions is encouraging.

Because snow substantially reduces the transmission of irradiance to the algal community, both the simulated and the observed rates of algal accumulation under ice with a 5-cm cover of snow were ~60% of the rate beneath clear ice (Fig. 5B, Table 3), demonstrating that algae growing in this environment were light limited. The impact of a 10-cm cover of snow on the rates of algal growth was even more severe. Under these conditions, the

Table 1. Biological coefficients and initial conditions used as defaults in the sea-ice model.

Name	Value	Units
Biochemical ratios (molar)		
C:N:Si:P	107:17:40:1	dimensionless
Half-saturation constants for algal growth		
NH_4	1	μM
NO_3	1	μM
$Si(OH)_4$	60	μM
PO_4	0.1	μM
Algal growth rate		
μ_0	0.8	d^{-1}
Q_{10}	1.9	dimensionless
Photophysiology		
$I_{k'\max}$	18	μEinst m^{-2} s^{-1}
A	1.7	dimensionless
B	0.12	dimensionless

Depth interval (m)	Salinity (‰)	Chl *a* (mg m^{-3})
0.0*H*–0.1*H*	8.0	1.0
0.1*H*–0.2*H*	6.3	1.0
0.2*H*–0.3*H*	5.6	1.0
0.3*H*–0.4*H*	5.3	1.0
0.4*H*–0.5*H*	5.2	1.0
0.5*H*–0.6*H*	5.1	1.0
0.6*H*–0.7*H*	4.9	1.0
0.7*H*–0.8*H*	4.8	1.0
0.8*H*–0.9*H*	4.8	1.0
0.9*H*–1.0*H*	6.7	1.0
H_p	34.5	1.0
Water column	34.5	0.5

Table 2. Environmental conditions used in simulations for McMurdo Sound, 1982.

	September			October			November			December		
	5	15	25	5	15	25	5	15	25	5	15	25
Air temp. (°C)	−30	−27	−23	−21	−19	−14	−10	−7	−5	−3	−2	−2
Clouds (0–10)	6.5	6.5	6.5	6.6	6.6	6.6	6.5	6.5	6.5	6.7	6.7	6.7
H_p (m)	0.6	0.6	0.6	0.6	0.6	0.6	0.6	0.6	0.6	0.6	0.6	0.6

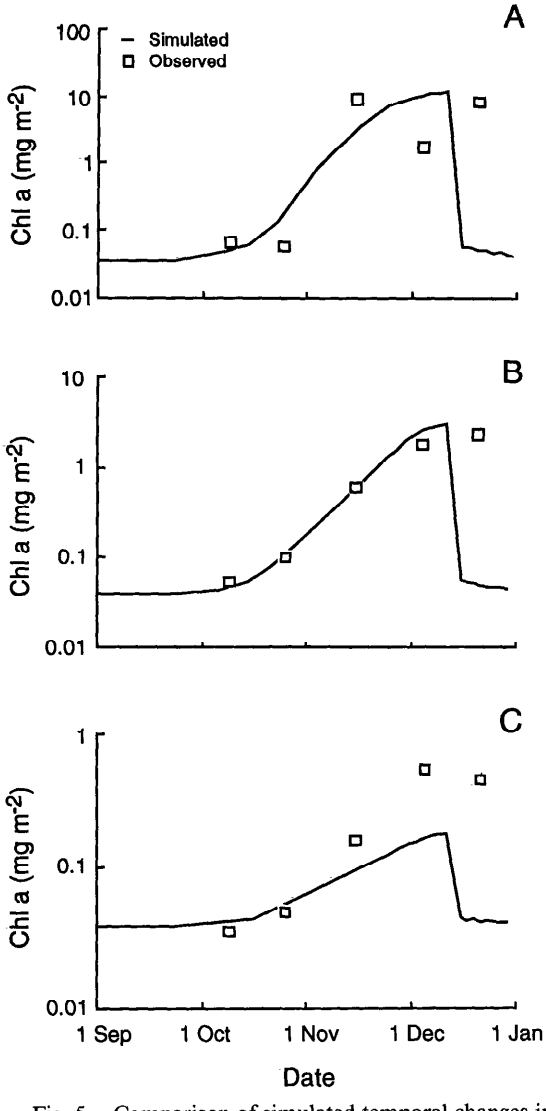

Fig. 5. Comparison of simulated temporal changes in Chl *a* standing crop in the congelation ice to observations made in McMurdo Sound in 1982 (data from Grossi et al. 1987) when snow cover was 0 cm (A), 5 cm (B), and 10 cm (C) thick.

observed rate of Chl *a* accumulation during the exponential phase of growth (between 24 October and 2 December) was 0.046 d^{-1} (Table 3)—extremely low compared to rates observed in the snow-free quadrat (0.16 d^{-1}). Standing crop at the peak of the bloom was also greatly reduced, only 7% of the maximum biomass observed beneath clear ice (Fig. 5C). These results support the conclusion that sea-ice production is controlled by snow depth via its influence on the ambient light field (Sullivan et al. 1985).

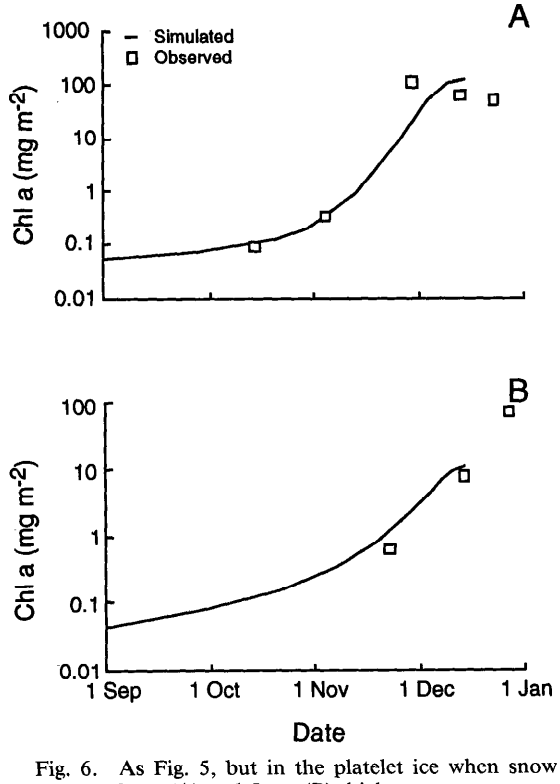

Fig. 6. As Fig. 5, but in the platelet ice when snow cover was 0 cm (A) and 5 cm (B) thick.

Table 3. Simulated and observed rates of Chl *a* accumulation (d^{-1}) in the congelation and platelet ice beneath 0, 5, and 10 cm of snow calculated for specified time intervals from Chl *a* standing crops.

Snow (cm)	Congelation ice		Platelet ice		Time interval
	Sim.	Obs.	Sim.	Obs.	
0	0.160	0.159			9 Oct–24 Nov
0			0.015	0.014	9 Oct–24 Nov
5	0.094	0.091			9 Oct–11 Dec
5			0.188*	0.213*	17 Nov–11 Dec
10	0.029	0.046			9 Oct–3 Dec

* Relatively higher accumulation rates are due in part to lateness of initial in situ Chl *a* measurement (17 November).

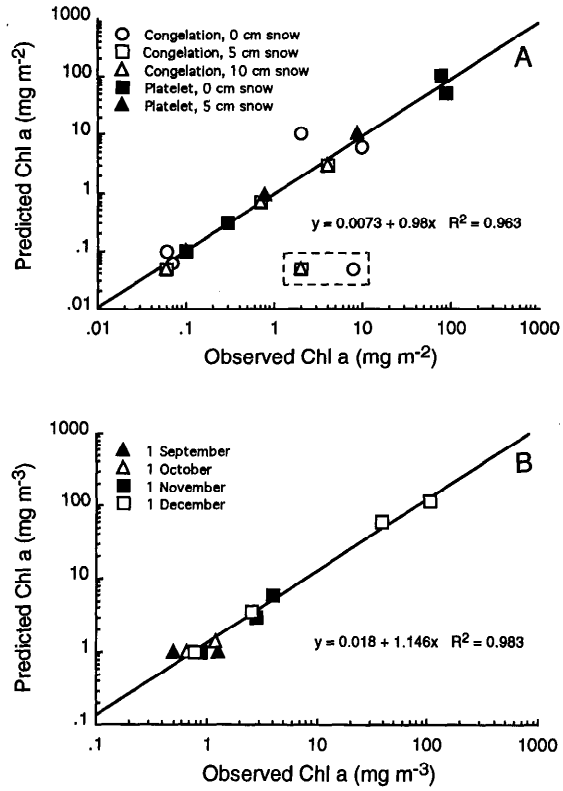

Fig. 7. Regression of predicted against observed integrated Chl *a* standing crop in the congelation and platelet ice (A) and Chl *a* concentrations obtained from profiles through the congelation ice (B). Observations were made in McMurdo Sound in 1982 beneath snow-free ice.

Interestingly, despite melting at the lower sea-ice surface, observed Chl *a* concentrations in the congelation ice remained high until the end of December—a phenomenon not predicted by the model (Figs. 5 and 6). This phenomenon was due to the growth of an anomalous microalgal "strand" community (*see* figure 3 of Grossi et al. 1987) composed primarily of the diatom *Berkeleyii* sp., which remained attached to the congelation ice after ice melt began. Because the model assumes that any biomass associated with a given layer of ice is lost as that layer melts, by late December the model predicted a severe decline in Chl *a* in the congelation ice which was not observed in 1982 (Fig. 5), resulting in the outlying points identified in Fig. 7A. It should be noted that strand communities are uncommon in McMurdo Sound, and the observed increase in algal abundance contrasts with the decline in algal biomass generally reported between middle and late December.

Simulated vertical distributions of Chl *a* also show good agreement with profiles obtained from congelation-ice cores beneath the snow-free quadrat (Fig. 7B). On 1 September, Chl *a* concentrations were ~1 mg m^{-3} and constant with depth in both observed and simulated profiles. Algal growth was sluggish due to the combined effects of extremely high salinity (consequently low ξ) and low light (low ρ) throughout most of the congelation ice (Fig. 8A). By 1 October, concentrations of Chl *a* had changed little in either the observed or simulated profiles. Although higher irradiance had caused an increase in ρ for the upper ice sheet, high salinity and low ξ (Fig. 8B) kept algal growth in check. In the lower congelation ice where ξ was higher, ρ was low due to light attenuation by the ice sheet. 1 November marked the first discernible increase in Chl *a* in both the observed and simulated profiles; this increase was restricted to the lower layers of the congelation ice. The light limitation term, ρ, had increased considerably in the upper ice (to 0.65, Fig. 8C), but algal growth was still inhibited by ξ (due to high salinity). Within the congelation-ice interior (at 1.5-m depth), both ρ and ξ were ~0.5, allowing algal growth at only 25% of the temperature-dependent maximum of 0.55 d^{-1}. In the lower congelation ice, where the largest increase in Chl *a* was observed, $\mu = 0.2$ d^{-1} ($\mu_{max} \cdot \rho \cdot \xi$). Between 1 November and 1 December, Chl *a* concentration had increased >20-fold in the lower congelation ice, to 92 mg m^{-3} in core samples, and to 108 mg m^{-3} in simulations—a difference of <15%. During this time, ρ had increased to

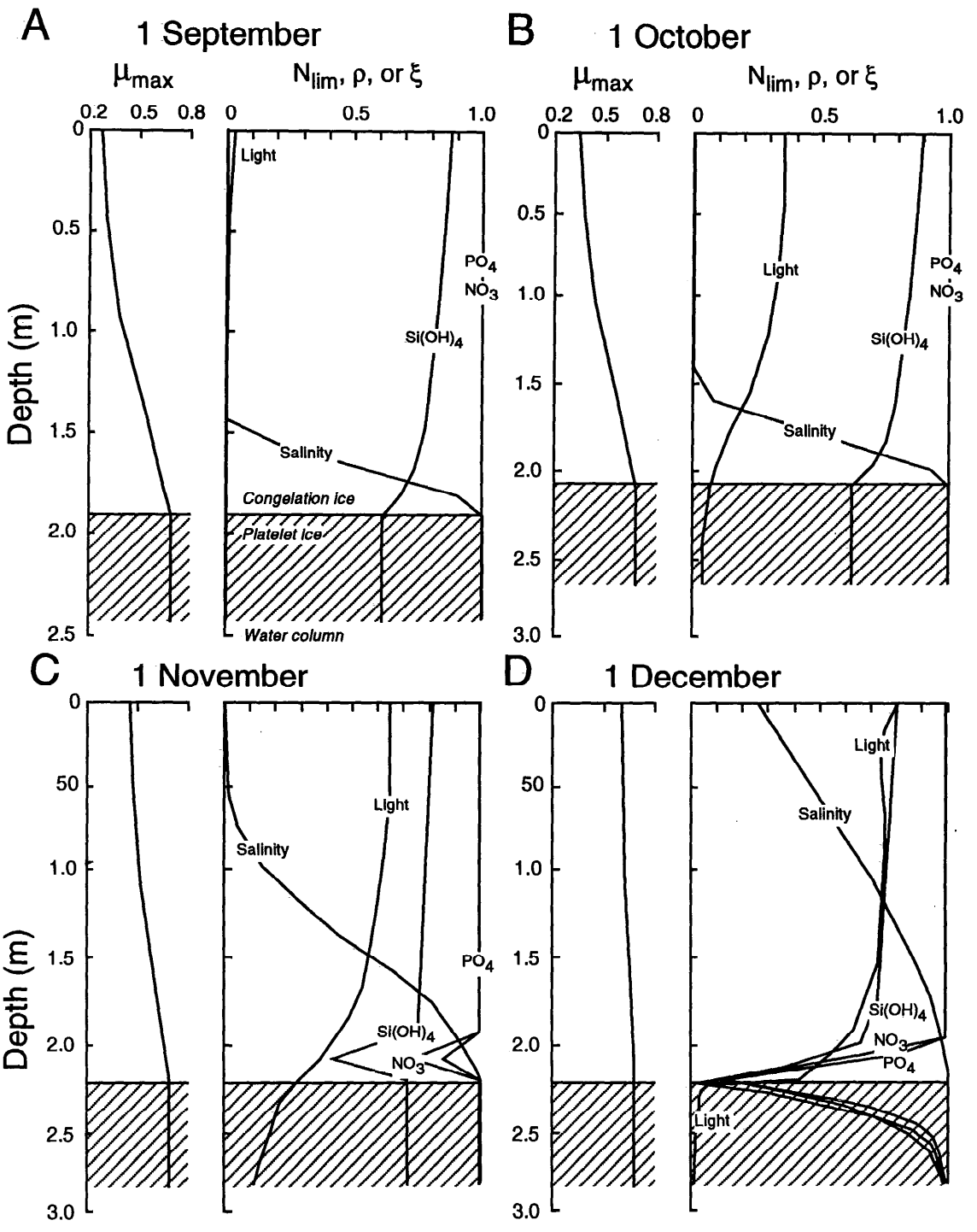

Fig. 8. Simulated profiles of temperature-specific maximum growth rate (μ_{max}) and reduction of microalgal growth by light (ρ), nutrients (N_{lim}), and salinity (ξ) in the congelation-ice and platelet-ice layer on dates indicated.

0.4 and μ to 0.3 d^{-1} (*see Fig. 10D*). By 1 December, the increased demand by this dense algal assemblage had depleted nutrients to the point where the system was nutrient limited in the lower congelation ice and the upper platelet ice. Self-shading reduced ρ to highly limiting levels throughout the rest of the platelet ice.

Profiles of μ_{max}, ρ, N_{lim}, and ξ imply that by 1 December (Fig. 8D) microalgal growth rates in the upper congelation ice were considerably higher than the static Chl *a* profiles observed in 1982 would indicate. As a rule, profiles of Chl *a* show little seasonal change in the upper ice (Arrigo et al. 1993*a*) despite the fact that μ is predicted to be at least 0.14 d^{-1} (Fig. 8D). This apparent anomaly was addressed in some detail by Arrigo et al. (1993*a*) who illustrated the effect of allowing algal biomass to increase in the upper congelation ice unchecked by microzooplankton grazers. They concluded that in the upper layers of the congelation ice (>20 cm above the lower margin), grazing by microzooplankton, whose numbers increase dramatically in this region of the ice sheet by December (Stoecker et al. 1990), maintains the algal population at relatively constant levels. Microzooplankton make up a much smaller proportion of the microbial population in the lower congelation-ice and the platelet-ice layer (Arrigo unpubl.) and do not appear to have a substantial influence on Chl *a* standing crop. Therefore, we were forced to assume that $g = 1$ for the upper ice sheet and $g = 0$ in the lower congelation-ice and platelet-ice layer. Preliminary simulations suggested that this constraint is extremely important, because when it was not invoked, Chl *a* concentrations increased throughout the upper congelation ice. The absence of this constraint resulted in shading of algae in the skeletal and the platelet layer, which reduced their growth rates and prevented the large increase in Chl *a* that is typically observed in that region by late November.

Sea ice is a complex environment where microalgal growth depends strongly on temporal variation in the physical, chemical, and biological characteristics of individual microhabitats within the ecosystem. Despite this fact, the model consistently yielded standing crops and Chl *a* profiles that were within 15% of observations for all three of the McMurdo Sound 1982 simulations. This agreement is especially encouraging, considering the potential for spatial variation in field measurements of algal biomass in sea ice and problems associated with artificially modifying snow cover (snow compaction, etc.). These results indicate that models of this type can be used to simulate the heterogeneity of a complex environment—a testament to the utility of growth formulations that can account for the variable physicochemical nature of many aquatic habitats.

Model sensitivity and behavior—The results presented above for McMurdo Sound in 1982 with a 0-, 5-, and 10-cm snow cover suggest that even a small amount of snow will have a considerable influence on algal bloom dynamics due to the snow's impact on light transmission (Arrigo et al. 1991). The high sensitivity of Chl *a* accumulation to variation in snow cover seen in simulations supports previous hypotheses that attribute the horizontal patchiness of algal distributions in sea ice to the presence of snow (Sullivan et al. 1985). Our results suggest that snow depths >10 cm will reduce light to the point that no net algal growth will occur. As a result, in fast-ice regions where snow accumulates and remains intact for long periods of time, sea-ice microalgal blooms will probably not develop. However, in regions where snowfall is low, where winds sweep the sea-ice surface relatively clear of snow, or where pack ice is dispersed enough to let in light, ice algae are likely to bloom.

The effect of temperature on bloom dynamics was tested by increasing or decreasing by 3° (~1.5 SD from the mean air temperature in McMurdo Sound between 1977 and 1990) the temperature used in the McMurdo Sound 1982 simulation for snow-free ice. Temperature has two primary effects on algal bloom dynamics in sea ice, and the two seem to offset each other over the course of a growth season. Initially, increased air temperature translates into slightly higher temperatures in the bottom 20 cm of the ice sheet (where >95% of the microalgal biomass resides), resulting in elevated growth rates and more rapid Chl *a* accumulation (Fig. 9A). The peak standing crop achieved under all temperature conditions varied between 5 and 10 mg Chl *a* m^{-2}. Eventually, however, warmer temperatures elicit earlier melting of sea ice and a loss of microalgal biomass from the ice sheet. For a short

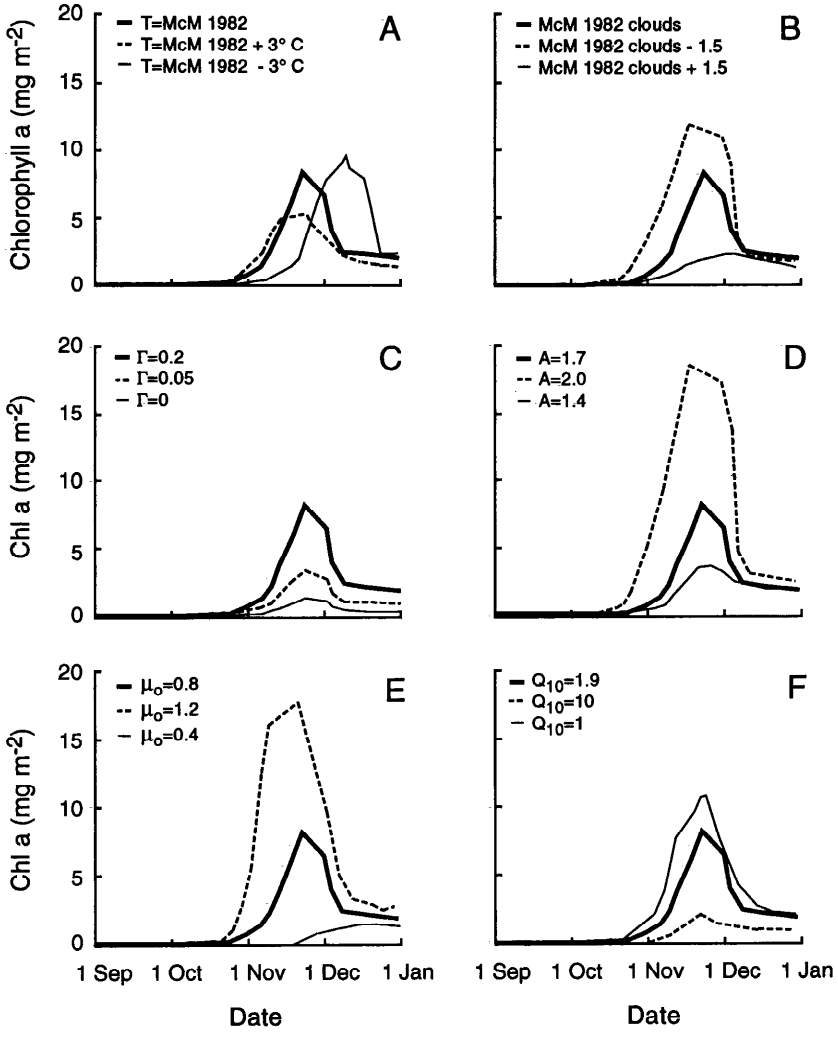

Fig. 9. The sensitivity of algal bloom dynamics to changes in (A) air temperature (McM 1982 is the air temperature for McMurdo Sound in 1982), (B) cloud cover, (C) nutrient transport coefficient (Γ, $m^2\ d^{-1}$), (D) I_k' parameter A, (E) μ_0, and (F) Q_{10}.

time, accumulation of new biomass nearly equals the loss due to sea-ice degradation, and standing crop levels off. Within a few days, however, algal losses during accelerated ice melt are too rapid for new growth to keep up, and standing crop declines precipitously. A seasonally constant 3°C increase in air temperature resulted in a 2-week shortening of the algal growth season in sea ice.

A number of global climate models predict at least a 3°C increase in atmospheric temperatures at high latitudes by the year 2020 due to the increased abundance of greenhouse gasses such as CO_2, chlorofluorocarbons, and methane. If this were to occur, our results suggest that total sea-ice production would be greatly reduced, and the timing of release of algal cells from the ice sheet would be accelerated, perhaps with serious repercussions for those polar species that rely on ice algal production for their nutrition. These include a variety of krill (Stretch et al. 1988) and other arthropod life stages (Hoshiai et al. 1987), as well as nearshore benthic communities (Dayton et al. 1986). It is possible, however, that early degradation of the sea-ice habitat could increase the length of the growth season for phytoplankton, thereby increasing production

in the marginal ice-edge zone. If this is the case, regional primary production could remain unchanged or even increase (although the species composition of the primary producers may be altered).

Like snow cover, increased cloudiness reduces the amount of irradiance reaching the algal community. When cloud cover measured in McMurdo Sound in 1982 was decreased by 1.5 units (~1.5 SD from the mean cloud cover in McMurdo Sound between 1977 and 1990) throughout the simulation, standing crop at the peak of the bloom increased 41%, from 8.2 to 11.6 mg Chl *a* m^{-2} (Fig. 9B). Similarly, increasing cloud cover by 1.5 units resulted in a 49% decrease in standing crop (to 4.2 mg Chl *a* m^{-2}), demonstrating the extreme light-limited nature of sea-ice ecosystems. Heavier cloud cover also delayed the onset of the bloom by ~1 week. Because monthly climatological data were interpolated to describe environmental conditions on a daily basis in simulations, the model was run with every day cloudy to some degree. The use of cloud climatologies would be a problem if there were a significant percentage of clear days in McMurdo Sound during the spring bloom. However, 14 yr of atmospheric data from McMurdo Sound (published in the *Antarctic Journal of the United States* for the years 1977 to 1989) reveal that 83% of the days were partly cloudy or cloudy between 1 September and 31 December (25.2 ± 4.2 d $month^{-1}$), with only 5.1 ± 4.0 clear days per month. In regions where clear days are more prevalent, a more rigorous description of cloud cover would be necessary; for our model of McMurdo Sound, monthly climatologies appear to be sufficient.

The flux of nutrients from the water column, through the platelet layer, and to the algal community has been described in the model in terms of a transport coefficient, Γ, which is analogous to the eddy diffusion coefficient, *K* (m^2 d^{-1}). Both *K* and Γ describe the rate of mixing between adjacent vertical fluid layers, although by different mechanisms. In McMurdo Sound, Γ has been shown to vary from 0.05 to 0.37 m^2 d^{-1} as a function of tidal height (Arrigo unpubl.). Model results suggest that the sea-ice ecosystem is nutrient-sufficient (i.e. the system is light limited) when Γ is held constant at values ≥ 0.2 m^2 d^{-1} (Fig. 9C). Reducing Γ to 0.05 m^2 d^{-1} for the duration of the simulation results in moderate nutrient limitation for the congelation-ice community, and, consequently, rates of Chl *a* accumulation are reduced. Peak standing crop under these conditions reached only 3.6 mg Chl *a* m^{-2}, 44% of the value in the default simulation. Reducing Γ further (to 0 m^2 d^{-1}) results in extreme nutrient limitation. In this case, nutrient resupply has been completely shut down, and the algal community is forced to subsist on whatever nutrients were available at the start of the simulation. The peak Chl *a* standing crop under this condition reached only 1.4 mg Chl *a* m^{-2}. In the present form of the model, Γ is held constant for the duration of each simulation. However, the results presented above imply that the model could be made more realistic by driving Γ empirically as a function of current velocity at the platelet ice–seawater interface.

Because sea ice is predominantly a light-limited system, algal bloom dynamics are particularly sensitive to the coefficients used to describe the relationship between I_k' and PUR. The default coefficients ($A = 1.7$, $B = 0.12$, and $I_{k'\max} = 18$ μEinst m^{-2} s^{-1}) used in Eq. 13 provided the best fit to the data shown in Fig. 2 (sum of squares, $R^2 = 0.72$) and resulted in excellent agreement between model results and observed algal bloom dynamics in McMurdo Sound in 1982. Alternative sets of I_k' coefficients fit the data nearly as well (Table 4) but yielded poor model results (Fig. 9D). For example, when $A = 2.0$, $B = 0.12$, and $I_{k'\max} = 18$ μEinst m^{-2} s^{-1}, the resulting $R^2 = 0.71$, similar to the fit provided by the default coefficients. When these were used as input to the model, the maximum standing crop of Chl *a* reached 19.1 mg m^{-2}, a factor of 2.1 greater than the standing crop predicted by the default values for *A*, *B*, and $I_{k'\max}$ (Table 4). Similarly, if $A = 1.4$, $B = 0.12$, and $I_{k'\max} = 18$, then $R^2 = 0.70$ and standing crop attained only 4.4 mg Chl *a* m^{-2}, a factor of >2.00 lower than the standing crop predicted by the default values. Increasing I_k' would also be expected to delay the Chl *a* peak during the simulated microalgal bloom. However, this was not observed, because the timing of the Chl *a* peak was also influenced by sea-ice melt and the associated loss of biomass due to sinking. These results underscore the extreme care that must be taken when estimating coefficients used in the I_k' model.

The growth rate of polar microalgae at 0°C

Table 4. The fit (R^2) and simulated peak Chl *a* standing crops for a variety of coefficients input to the equation: $I_k' = I_k'_{max}[1 + A \exp(-B \cdot PUR)]^{-1}$.

$I_k'_{max}$	A	B	R^2	Chl *a* (mg m^{-2})
18	2.00	0.12	0.71	19.1
17	1.70	0.12	0.71	15.4
17	1.55	0.12	0.71	9.7
18	1.70	0.12	0.72	9.2
20	2.00	0.12	0.69	8.1
18	1.40	0.12	0.70	4.4
20	1.70	0.12	0.67	4.3

computed from a variety of sources (Grossi et al. 1984; Spies 1987) varies from 0.4 to 1.2 d^{-1}, substantially different from the estimate of 0.85 d^{-1} proposed by Eppley (1972). Simulations indicate that rates of algal accumulation are highly sensitive to variations in μ_0 (Fig. 9E). For instance, increasing μ_0 from 0.85 to 1.2 d^{-1} resulted in a rapid accumulation of algal material, which reached 16 mg Chl *a* m^{-2} by 16 November. Reducing μ_0 to 0.4 d^{-1} yielded a peak standing crop of 1.5 mg Chl *a* m^{-2}, only 16% of the 9.2 mg Chl *a* m^{-2} obtained when $\mu_0 = 0.85$ d^{-1}. Because the use of μ_0 at variance with the estimate of Eppley (1972) resulted in such poor model performance, it appears that the thermodynamic constraints which form the basis of the Eppley coefficient μ_0 may apply to psychrophilic sea-ice microalgae as well as to temperate phytoplankton.

Estimates of Q_{10} for ice-algal photosynthesis at low temperatures vary widely, from 1 to >20 (Palmisano et al. 1985; Priscu et al. 1989). Because sea-ice T is < -1.8°C and decreases toward the upper sea-ice surface, increasing the Q_{10} value in simulations will decrease μ. Reducing Q_{10} from 1.88 (Eppley 1972) to 1.0 (algal growth is insensitive to temperature) resulted in a modest increase in the peak Chl *a* standing crop from 8.2 to 10.5 mg m^{-2} (Fig. 9F). Increasing Q_{10} to 10, however, substantially lowered the peak level of accumulated biomass to 3.2 mg Chl *a* m^{-2}. Although a Q_{10} value of 1.88 (Eppley 1972) results in good agreement between simulated and observed algal bloom dynamics, simulations suggest that values ranging from 1 to 5 would perform almost equally well. This somewhat surprising result is due to the interacting influences of temperature and salinity. At temperatures < -7°C, salinity ≥ 100‰, and $\mu = 0$. Obviously, Q_{10} is irrelevant to μ at these temperatures. However, even at temperatures between -7°C and -1.86°C, salinity exerts a stronger influence on μ than does temperature (Aletsee and Jahnke 1992; Arrigo et al. 1993*a*), reducing the impact of Q_{10} variations on μ. Because temperature is so dynamic in the upper congelation ice, relaxing the grazing constraint (all net production is now grazed in the upper ice) could slightly alter the Q_{10} response shown in Fig. 9F. The effect is likely to be marginal, however, because algal growth rates in the upper ice are low from September to mid-November due to high salinity and after mid-December due to nutrient depletion, limiting their potential response to temperature.

The I_k' *model*—When I_k' for sea-ice microalgae is plotted against $\log_{10}$(PUR), the relationship is sigmoidal in shape (Fig. 2B), with I_k' exhibiting an upper and lower asymptote at the extremes of PUR. This finding implies that sea-ice microalgae have a finite range of irradiances over which they are able to photoacclimate, a characteristic that some have speculated is genetically predetermined (Cullen 1990; *but see* Lizotte and Sullivan 1991). The lower irradiance threshold is shown with particular clarity in Fig. 1B, where the minimum value for I_k' is 4 μEinst m^{-2} s^{-1} despite microalgae being exposed to values of PUR as low as 0.2 μEinst m^{-2} s^{-1} for several days (Arrigo unpubl.). The higher than expected I_k' may reflect a retention of excess photosynthetic capacity as an adaptation to low but variable light levels or a biophysical constraint to increasing photosynthetic efficiency (Arrigo et al. 1993*b*). The maximum PUR to which sea-ice microalgae photoacclimate ranged from 20 to 25 μEinst m^{-2} s^{-1}. These low values contrast markedly with temperate phytoplankton, which may exhibit values for I_k in excess of 300 μEinst m^{-2} s^{-1} (Sakshaug et al. 1989) corresponding approximately to an I_k' of 150 μEinst m^{-2} s^{-1}. Light shift experiments performed on microalgae collected from McMurdo Sound support the hypothesis that these sea-ice species are constrained in their ability to photoacclimate to very high or very low irradiance. Ice microalgae exposed to irradiances as high as 600 μEinst m^{-2} s^{-1} underwent a variety of physiological changes during acclimation, including a decrease in Chl *a* per cell, an alteration of pigment ratios, and increased assimilation rate, yet I_k' reached a

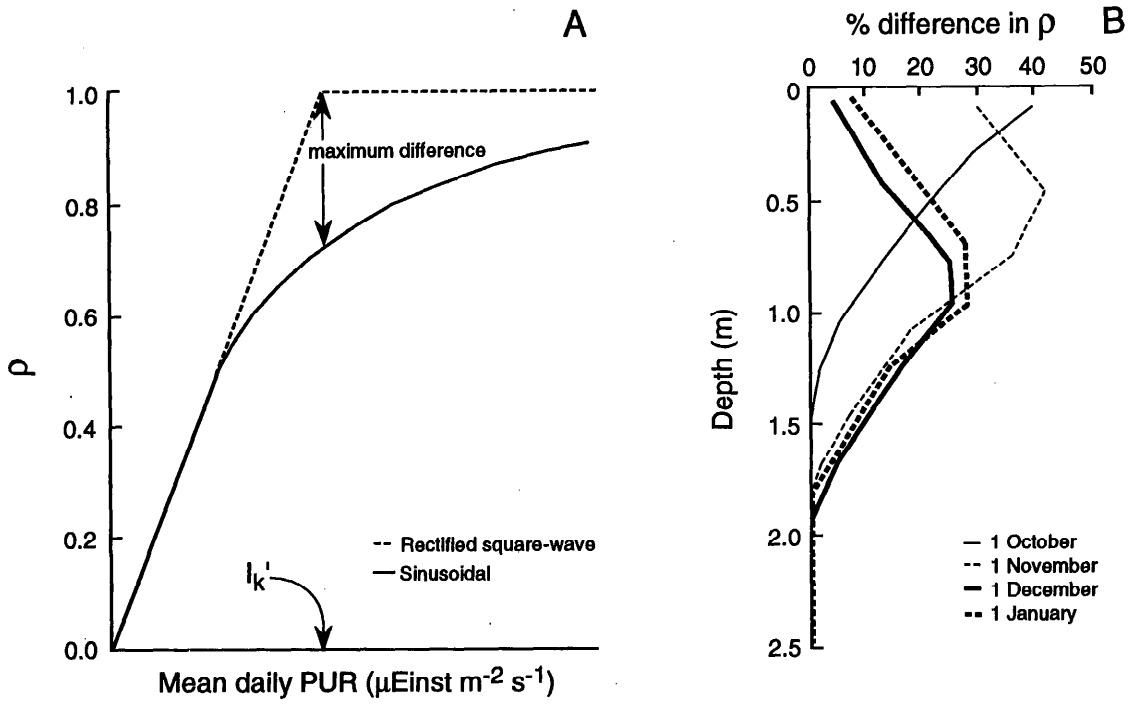

Fig. 10. A. Comparison of the light-limitation coefficient, ρ, as estimated by both the sinusoidal and rectified square-wave schemes for McMurdo Sound in 1982 beneath snow-free ice. At values of mean daily PUR up to $\sim I_k'/2$, the sinusoidal and rectified square-wave schemes are in perfect agreement. As the mean daily PUR increases, however, the two predictions of light limitation diverge, with the difference maximal when PUR = I_k'. B. The percentage difference in predicted light limitation [(rectified-diel)/rectified] between the sinusoidal and rectified square-wave schemes as a function of depth in the congelation ice.

maximum value of only 20 μEinst m^{-2} s^{-1} (Robinson 1992). Figure 1B suggests that I_k' for bottom-ice microalgae is most dynamic when PUR varies from 5 to 20 μEinst m^{-2} s^{-1}, a typical range for under-ice irradiance in McMurdo Sound during austral spring (Palmisano et al. 1987*a*; SooHoo et al. 1987; Arrigo et al. 1991).

When microalgal growth has been modeled previously, ambient irradiance has often been held constant throughout the light cycle at a level considered to represent the daily mean (Sakshaug et al. 1991; Kiefer and Cullen 1991). In this rectified square-wave scheme, irradiance oscillates between total darkness at night and the daily mean, with no transitional period. Although this scheme is artificial, it has the advantage of mathematical simplicity. Incorporation of realistic diel changes in $E_d(\lambda)$ into models of microalgal growth should result in significant improvement over previous methods that ignore daylength or that use rectified square-wave functions to describe daily irradiance (Platt et al. 1990; Platt and Sathyendranath 1991).

The comparison of predictions of light limitation (ρ) calculated with our sinusoidal scheme with the rectified square-wave scheme suggests that under case 1 or case 3 conditions, both the square-wave and sinusoidal formulations are in good agreement. However, for case 2, the rectified square-wave scheme overestimates the algal growth rate relative to the sinusoidal method by calculating a ρ that is too large. This problem becomes increasingly serious as the mean daily irradiance approaches I_k'. For example, in the square-wave scheme, light levels are always saturating and $\rho = 1$. However, in the sinusoidal scheme, PUR varies about the mean irradiance on a diel basis, and therefore light is at subsaturating levels for part of the day, i.e. $\rho < 1$. Figure 10A illustrates a detailed comparison of ρ calculated from either the sinusoidal or square-wave schemes as a function of increasing mean daily PUR for case 2. At values of PUR up to $\sim I_k'/2$, the

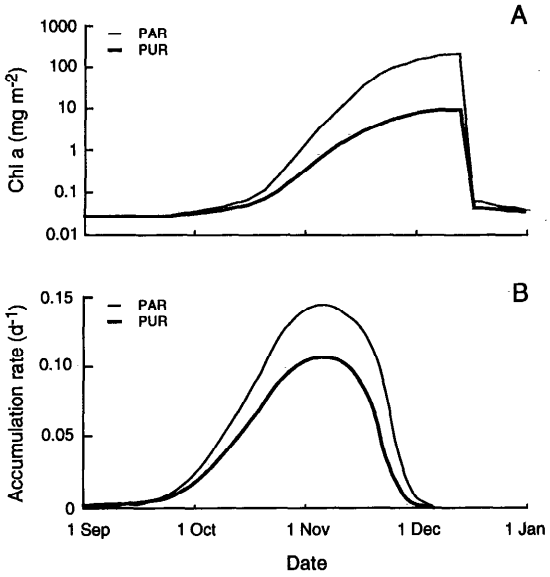

Fig. 11. Comparison of simulated standing crop (A) and Chl *a* accumulation rate (B) obtained when PAR was used as input to the I_k model and PUR was used as input to the I_k' model.

sinusoidal and square wave are in perfect agreement. As mean daily PUR increases, however, the two predictions of light limitation diverge, with the difference maximal when PUR = i_k'.

In practice, the divergence of the two approaches would be highly time- and depth-dependent (Fig. 10B) and would be maximal at depths where PUR = I_k'. Because it is generally assumed that the value for I_k' expressed by an algal assemblage is a reflection of its light history (Falkowski and Owens 1980), the rectified square-wave scheme would be expected to severely overpredict rates of algal growth, while the sinusoidal scheme should result in the best estimate of light-limited algal growth under most circumstances.

Sathyendranath et al. (1989) showed that errors in excess of 50% can result when estimates of primary production are made without consideration of the spectral irradiance distribution. A comparison of simulations obtained separately, using PAR as input to the I_k model and PUR to the I_k' model (for the McMurdo Sound 1982 snow-free condition), demonstrates the importance of basing estimates of light-dependent algal growth on the spectral-dependent quantity PUR, particularly when the spectral characteristics of the downwelling irradiance are changing rapidly with depth. The peak simulated standing crops obtained with PAR were more than an order of magnitude higher than those based on PUR, reaching 127.1 and 9.2 mg Chl *a* m^{-2}, respectively (Fig. 11A). Rates of Chl *a* accumulation based on PAR were as high as 0.15 d^{-1} (Fig. 11B), >37% higher than corresponding rates obtained when PUR was used.

Simulated algal growth rates based on PAR are overestimates because they neglect the spectral shifts that occur as irradiance propagates through the ice sheet and, more importantly, as the optimal blue and red wavelengths are selectively absorbed within the algal community. These spectral shifts drastically alter the proportion of PAR that can be absorbed by photosynthetic pigments (i.e. PUR) for algae at greater depths within the ice sheet. For example, the spectral irradiance distribution at the sea-ice surface (Fig. 12A) is such that ~50% of the light is in the form of PUR (Fig. 12D), based on the spectral absorption properties of the microalgae (*see Eq. 9, Fig. 12A*). Irradiance that is not reflected from the sea-ice surface is transmitted through the ice sheet, where it is diminished in magnitude (not shown) and shifted toward 470 nm (Fig. 12B) as the bulk of the red light is attenuated by sea-ice crystals. This spectral narrowing results in an irradiance distribution that is similar in shape to the absorption spectrum of ice microalgae and is therefore readily absorbed by photosynthetic pigments (Fig. 12C). Consequently, PUR, expressed as a percentage of PAR, increases with depth within the ice sheet (Fig. 12D), reaching a peak of 60% (this increase in PUR with depth relative to PAR is also observed in the water column where pigment concentrations are low).

Note, however, that although PUR as a percentage of PAR increases with depth in pigment-free sea ice, PUR is substantially less than PAR at all depths. As the irradiance reaches the algal community located in the lower layers of the congelation ice and upper platelet ice (Fig. 12E), photosynthetic pigments selectively absorb the bulk of the blue (410–490 nm) and red (660–690 nm) wavelengths (Fig. 12C), transmitting only the poor-

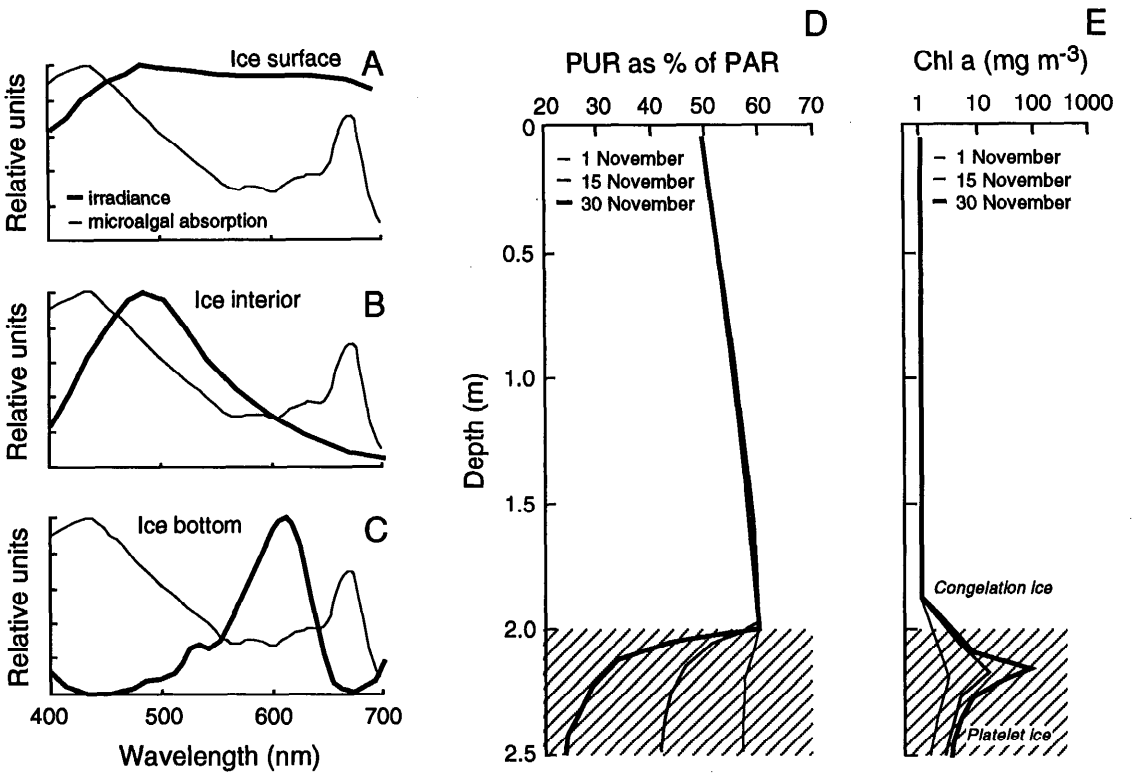

Fig. 12. The spectral irradiance and microalgal absorption spectra from which PUR was calculated for the sea-ice surface (A), interior (B), and bottom (C) for McMurdo Sound in 1982, beneath snow-free ice. D. Simulated seasonal changes in the vertical distribution of PUR (as a percentage of PAR) in the congelation and platelet ice. E. Simulated seasonal changes in the vertical distribution of Chl *a* in the congelation and platelet ice.

er quality green light (580–620 nm). Because algal pigments do not absorb well at these wavelengths, PUR declines rapidly to <25% of PAR within the confines of the algal community (Fig. 12D). The disparity between PUR and PAR under these conditions is cause for the large differences in the predicted algal growth and Chl *a* accumulation rates evident in the simulations.

References

ALETSEE, L., AND J. JAHNKE. 1992. Growth and productivity of the psychrophilic marine diatoms *Thalassiosira antarctica* Comber and *Nitzschia frigida* Grunow in batch cultures at temperatures below the freezing point of sea water. Polar Biol. **11:** 643–647.

ARRIGO, K. R., J. N. KREMER, AND C. W. SULLIVAN. 1993*a*. A simulated Antarctic fast-ice ecosystem. J. Geophys. Res. **98:** 6929–6946.

———, D. H. ROBINSON, AND C. W. SULLIVAN. 1993*b*. A high resolution study of the platelet ice ecosystem in McMurdo Sound, Antarctica: Photosynthetic and bio-optical characteristics of a dense microalgal bloom. Mar. Ecol. Prog. Ser. **98:** 173–185.

———, AND C. W. SULLIVAN. 1992. The influence of salinity and temperature covariation on the photophysiological characteristics of Antarctic sea ice microalgae. J. Phycol. **28:** 746–756.

———, ———, AND J. N. KREMER. 1991. A bio-optical model of antarctic sea ice. J. Geophys. Res. **96:** 10,581–10,592.

AZAM, F., B. B. HEMMINGSEN, AND B. E. VOLCANI. 1974. Role of silicon in diatom metabolism. 6. Silicic acid transport and metabolism in the heterotrophic diatom *Nitzschia alba*. Arch. Mikrobiol. **97:** 103–114.

BATES, S. S., AND G. F. COTA. 1986. Fluorescence induction and photosynthetic responses of Arctic ice algae to sample treatment and salinity. J. Phycol. **22:** 421–429.

BLACKMAN, F. F. 1905. Optima and limiting factors. Ann. Bot. **19:** 281–295.

CULLEN, J. J. 1990. On models of growth and photosynthesis in phytoplankton. Deep-Sea Res. **37:** 667–683.

DAYTON, P. K., AND OTHERS. 1986. Distribution patterns

of benthic microalgal standing stock at McMurdo Sound, Antarctica. Polar Biol. **6:** 207–213.

DIECKMANN, G. S., K. R. ARRIGO, AND C. W. SULLIVAN. 1992. A high resolution sampler for nutrient and chlorophyll *a* profiles of the sea ice platelet layer and underlying water column below fast ice in polar oceans: Preliminary results. Mar. Ecol. Prog. Ser. **80:** 291–300.

EPPLEY, R. W. 1972. Temperature and phytoplankton growth in the sea. Fish. Bull. **70:** 1063–1085.

FALKOWSKI, P. G. 1975. Nitrate uptake in marine phytoplankton: Comparison of half saturation constants from seven species. Limnol. Oceanogr. **20:** 412–417.

———. 1981. Light-shade adaptation and assimilation numbers. J. Plankton Res. **3:** 203–215.

———, AND T. G. OWENS. 1980. Light-shade adaptation: Two strategies in marine phytoplankton. Plant Physiol. **66:** 592–595.

GEIDER, R. J. 1992. Respiration: Taxation without representation?, p. 333–360. *In* P. G. Falkowski and A. D. Woodhead [eds.], Primary productivity and biogeochemical cycles in the sea. Plenum.

GOSSELIN, M., L. LEGENDRE, S. DEMERS, AND R. G. INGRAM. 1985. Responses of sea-ice microalgae to climatic and fortnightly tidal energy inputs (Manitounuk Sound, Hudson Bay). Can. J. Fish. Aquat. Sci. **42:** 999–1006.

GRANT, W. S., AND R. A. HORNER. 1976. Growth responses to salinity variation in four Arctic ice diatoms. J. Phycol. **12:** 180–185.

GROSSI, S. M., S. T. KOTTMEIER, R. L. MOE, G. T. TAYLOR, AND C. W. SULLIVAN. 1987. Sea ice microbial communities 6. Growth and primary production in bottom ice under graded snow cover. Mar. Ecol. Prog. Ser. **35:** 153–164.

———, ———, AND C. W. SULLIVAN. 1984. Sea ice microbial communities. 3. Seasonal abundance of microalgae and associated bacteria, McMurdo Sound, Antarctica. Microb. Ecol. **10:** 231–242.

HARDING, L. W., B. B. PREZELIN, B. M. SWEENEY, AND J. L. COX. 1982. Diel oscillations of the photosynthesis-irradiance (P-I) relationship in natural assemblages of phytoplankton. Mar. Biol. **67:** 167–178.

HOSHIAI, T., A. TANIMURA, AND K. WATANABE. 1987. Ice algae as food of an Antarctic ice-associated copepod, *Paralabidocera antarctica* (I. C. Thompson). Proc. NIPR Symp. Polar Biol. **1:** 105–111.

JOHNSEN, G., AND E. N. HEGSETH. 1991. Photoadaptation of sea ice microalgae in the Barents Sea. Polar Biol. **11:** 179–184.

KIEFER, D. A., AND J. J. CULLEN. 1991. Phytoplankton growth and light absorption as regulated by light, temperature, and nutrients. Polar Res. **10:** 163–172.

———, AND B. G. MITCHELL. 1983. A simple, steady state description of phytoplankton growth based on absorption cross section and quantum efficiency. Limnol. Oceanogr. **28:** 770–776.

KOTTMEIER, S. T., S. M. GROSSI, AND C. W. SULLIVAN. 1987. Sea ice microbial communities. 8. Bacterial production in annual sea ice of McMurdo Sound, Antarctica. Mar. Ecol. Prog. Ser. **35:** 175–186.

LAWS, E. A., AND T. T. BANNISTER. 1980. Nutrient- and light-limited growth of *Thalassiosira fluviatis* in continuous culture, with implications for phytoplankton growth in the ocean. Limnol. Oceanogr. **25:** 457–473.

LIZOTTE, M. P., AND C. W. SULLIVAN. 1991. Photosynthesis-irradiance relationships in microalgae associated with Antarctic pack ice: Evidence for in situ activity. Mar. Ecol. Prog. Ser. **71:** 175–184.

MADDUX, W. S., AND R. F. JONES. 1964. Some interactions of temperature, light intensity, and nutrient concentration during continuous culture of *Nitzschia closterium* and *Tetraselmis* sp. Limnol. Oceanogr. **9:** 79–86.

MEGURO, H., K. ITO, AND K. FUKUSHIMA. 1967. Ice flora (bottom type): A mechanism of primary production in polar seas and the growth of diatoms in sea ice. Arctic **20:** 114–133.

MONOD, J. 1942. Recherches sur la croissance des cultures bacteriennes. Herman et Cie.

MOREL, A. 1978. Available, usable, and stored radiant energy in relation to marine photosynthesis. Deep-Sea Res. **25:** 673–688.

———. 1991. Light and marine photosynthesis: A spectral model with geochemical and climatological implications. Prog. Oceanogr. **26:** 263–306.

PALMISANO, A. C., J. B. SOOHOO, R. L. MOE, AND C. W. SULLIVAN. 1987*a*. Sea ice microbial communities 7. Changes in under-ice spectral irradiance during the development of Antarctic sea ice microalgal communities. Mar. Ecol. Prog. Ser. **35:** 165–173.

———, ———, AND C. W. SULLIVAN. 1985. Photosynthesis-irradiance relationships in sea ice microalgae from McMurdo Sound, Antarctica. J. Phycol. **21:** 341–346.

———, ———, AND ———. 1987*b*. Effects of four environmental variables on photosynthesis-irradiance relationships in Antarctic sea-ice microalgae. Mar. Biol. **94:** 299–306.

———, AND C. W. SULLIVAN. 1983. Sea ice microbial communities (SIMCO). 1. Distribution, abundance, and primary production of ice microalgae in McMurdo Sound, Antarctica in 1980. Polar Biol. **2:** 171–177.

PLATT, T., C. L. GALLEGOS, AND W. G. HARRISON. 1980. Photoinibition of photosynthesis in natural assemblages of marine phytoplankton. J. Mar. Res. **38:** 686–701.

———, AND S. SATHYENDRANATH. 1991. Biological production models as elements of coupled, atmosphere-ocean models for climate research. J. Geophys. Res. **96:** 2585–2592.

———, ———, AND P. RAVINDRAN. 1990. Primary production by phytoplankton: Analytic solutions for daily rates per area of water surface. Proc. R. Soc. Lond. Ser. B **241:** 101–111.

PRISCU, J. C., A. C. PALMISANO, L. R. PRISCU, AND C. W. SULLIVAN. 1989. Temperature dependence of inorganic nitrogen uptake and assimilation in Antarctic sea-ice microalgae. Polar Biol. **9:** 443–446.

REDFIELD, A. C. 1958. The biological control of chemical factors in the environment. Am. Sci. **46:** 205–221.

RILEY, G. A. 1946. Factors controlling phytoplankton populations on the Georges Bank. J. Mar. Res. **6:** 54–73.

RIVKIN, R. B., AND M. PUTT. 1988. Seasonal pattern of diel periodicity in photosynthesis by polar phytoplankton: Species-specific responses. J. Phycol. **24:** 369–376.

ROBINSON, D. H. 1992. Photosynthesis in sea ice microalgae: Response to low temperatures and extremes of irradiance. Ph.D. thesis, Univ. Southern California. 357 p.

RYTHER, J. H. 1956. Photosynthesis in the ocean as a function of light intensity. Limnol. Oceanogr. **2:** 281–286.

SAKSHAUG, E., K. ANDRESEN, AND D. KIEFER. 1989. A steady state description of growth and light absorption in the marine planktonic diatom *Skeletonema costatum.* Limnol. Oceanogr. **34:** 198–205.

———, G. JOHNSEN, K. ANDRESEN, AND M. VERNET. 1991. Modeling of light dependent algal photosynthesis and growth: Experiments with the Barents Sea diatoms *Thalassiosira nordkenskioeldii* and *Chaetoceros furcellatus.* Deep-Sea Res. **38:** 415–430.

SATHYENDRANATH, S., T. PLATT, C. M. CAVERHILL, R. E. WARNOCK, AND M. R. LEWIS. 1989. Remote sensing of oceanic primary production: Computations using a spectral model. Deep-Sea Res. **36:** 431–453.

SHUTER, B. 1979. A model of physiological adaptation in unicellular algae. J. Theor. Biol. **78:** 519–552.

SMITH, R. C., B. B. PRÉZELIN, R. R. BIDIGARE, AND K. S. BAKER. 1989. Bio-optical modeling of photosynthetic production in coastal waters. Limnol. Oceanogr. **34:** 1524–1544.

SOMMER, U. 1986. Nitrate and silicate-competition among antarctic phytoplankton. Mar. Biol. **91:** 345–351.

SOOHOO, J. B., AND OTHERS. 1987. Spectral light absorption and quantum yield of photosynthesis in sea ice microalgae and a bloom of *Phaeocystis pouchetii* from McMurdo Sound, Antarctica. Mar. Ecol. Prog. Ser. **39:** 175–189.

SPIES, A. 1987. Growth rates of Antarctic marine phytoplankton in the Weddell Sea. Mar. Ecol. Prog. Ser. **41:** 267–274.

STOECKER, D. K., K. R. BUCK, AND M. PUTT. 1990. A flagellate and ciliate dominated microbial community in the land-fast ice. Antarct. J. U.S. **25:** 197–199.

STRETCH, J. J., AND OTHERS. 1988. Foraging behavior of antarctic krill *Euphausia superba* on sea ice microalgae. Mar. Ecol. Prog. Ser. **44:** 131–139.

SULLIVAN, C. W., A. C. PALMISANO, S. T. KOTTMEIER, S. M. GROSSI, AND R. MOE. 1985. The influence of light on growth and development of the sea-ice microbial community of McMurdo Sound, p. 78–83. *In* W. R. Siegfried et al. [eds.], Antarctic nutrient cycles and food webs. Springer.

WILLIAMS, P. J. LEB. 1973. The validity of the application of simple kinetic analysis to heterogeneous microbial populations. Limnol. Oceanogr. **18:** 159–164.

WROBLEWSKI, J. S. 1977. A model of phytoplankton plume formation during variable Oregon upwelling. J. Mar. Res. **35:** 357–394.

———, AND J. G. RICHMAN. 1987. The non-linear response of plankton to wind mixing events—implications for survival of larval northern anchovy. J. Plankton Res. **9:** 103–123.

YENTSCH, C. S. 1981. Vertical mixing, a constraint on primary production: An extension of the concept of an optimal mixing zone, p. 67–78. *In* Ecohydronymics. Proc. Int. Liege Colloq. Ocean Hydrodynamics. Elsevier.

Submitted: 19 January 1993
Accepted: 12 July 1993
Amended: 17 August 1993